BMC Medical Genomics

RESEARCH

Open Access

# Palmitoylation remodeling dictates HCC heterogeneity: implications for subtype-specific prognostication and targeting the YAP-RhoA axis

Boqun Xu[1,2†], Jialin Dai[3†] and Zhong Chen[1*]

**Abstract**

Palmitoylation, a critical post-translational modification mechanism, plays a pivotal role in hepatocellular carcinoma (HCC) tumorigenesis and progression. While multiple palmitoylated proteins have been reported to regulate HCC development, systematic characterization of palmitoylation-associated gene signatures and molecular subtyping based on these regulators remains unexplored. Integrated analysis of transcriptomic profiles enabled stratification of HCC into two distinct palmitoylation-associated molecular subtypes through unsupervised consensus clustering. These subtypes exhibited significant heterogeneity in clinical outcomes, tumor microenvironment features, and therapeutic vulnerabilities. A palmitoylation-related prognostic signature was constructed via LASSO-Cox regression. PAL1 showed a marked association with activated cell cycle programs, epithelial-mesenchymal transition (EMT), and WNT/β-catenin signaling. This subtype also correlated with elevated tumor mutation burden (TMB) and poorer patient prognosis. Conversely, PAL2 was closely associated with the expression of differentiation markers and upregulated lipid metabolic processes. Significantly, pronounced molecular divergence characterized the two PAL subtypes. Additionally, ARHGEF3 was critically identified as a key discriminator between the PAL subtypes, and its expression level was significantly correlated with patient prognosis in HCC. ARHGEF3 was upregulated in HCC and demonstrated functional potential to drive tumor cell proliferation and migration, potentially mediated by the YAP-RhoA signaling cascade. Collectively, this study identifies novel molecular biomarkers and thereby establishes a robust framework for clinical translation.

**Keywords** Hepatocellular Carcinoma, Palmitoylation, Molecular subtypes, ARHGEF3

†Boqun Xu and Jialin Dai contributed equally to this work.

*Correspondence:
Zhong Chen
chenz9806@163.com
[1]Department of Hepatobiliary Surgery, Affiliated Hospital of Nantong University, Nantong, Jiangsu Province 226100, China
[2]Rudong People's Hospital, Nantong, Jiangsu Province 226400, China
[3]Department of Pharmacy, Kunshan Hospital of Traditional Chinese Medicine, Kunshan 215300, China

## Introduction

Globally recognized as a major oncological challenge, hepatocellular carcinoma occupies the sixth position in global cancer incidence while demonstrating the third-highest fatality rate among malignant tumors. Epidemiological data indicates nearly one million newly confirmed cases emerge yearly, accompanied by mortality figures surpassing 800,000 individuals affected by this aggressive disease [1]. While progressive optimization of TNM classification systems for HCC variants and evolution of treatment protocols have been achieved, a substantial proportion of patients still exhibit poor responsiveness to conventional therapeutic approaches such as operative interventions, cytotoxic drug regimens, and molecular-targeted agents [2, 3]. This persistent clinical dilemma has driven intensified research efforts toward identifying innovative prognostic indicators and developing advanced molecular subtyping frameworks.

Protein S-palmitoylation, a reversible post-translational modification, is enzymatically regulated by zinc finger DHHC-containing (ZDHHC) protein family members, with the reverse reaction catalyzed by palmitoyl-protein thioesterases (PPTs) [4–6]. This dynamic modification modulates protein-protein interactions and signal transduction by altering biochemical properties of target proteins [7, 8]. Recent advances have unveiled its critical regulatory roles in tumorigenesis, where palmitoylation of PI4KIIα and NTSR-1 in breast cancer promotes tumor growth, while CD82 and integrin α6β4 palmitoylation in prostate cancer facilitates metastasis, with CD82 modification additionally driving hematologic tumor dissemination and angiogenesis [9–12]. Furthermore, palmitoylation critically influences tumor metabolism, exemplified by KRAS4A palmitoylation-mediated glycolytic regulation in pancreatic cancer and SLC1A3 palmitoylation-enhanced glutamate uptake in glioblastoma [13, 14]. Intriguingly, colorectal cancer studies demonstrate tumor-suppressive associations through Wnt2B, DR4, and ZDHHC9 palmitoylation, collectively underscoring the context-dependent complexity of palmitoylation in oncogenic processes [15–17]. The relationship between protein palmitoylation and tumor progression in HCC warrants focused attention. PCSK9, FASN, and AEG-1 have been reported to undergo palmitoylation modifications that directly regulate HCC progression [18–20].

However, the construction of a molecular subtyping framework based on palmitoylation-related genes that reflect clinical characteristics and prognosis in HCC remains an unmet need. Furthermore, the interplay between palmitoylation-associated genes and key tumor biological features—such as the tumor microenvironment and tumor mutational burden—has not been thoroughly investigated. These gaps highlight the innovative contribution and clinical translational value of this study.

To address this critical gap, we designed and executed a study integrating multi-omics bioinformatics analysis with systematic experimental validation. First, leveraging transcriptomic data from public cohorts, we performed unsupervised consensus clustering to stratify HCC into distinct palmitoylation-associated molecular subtypes (PAL1 and PAL2). We then thoroughly characterized these subtypes in terms of their prognostic relevance, genetic alterations, tumor microenvironment features, and therapeutic vulnerabilities. Subsequently, to translate these findings into a clinically applicable tool, we constructed a palmitoylation-related prognostic signature using LASSO-Cox regression and validated its predictive power in independent multicenter cohorts. Finally, to move beyond computational associations and establish causality, we selected key candidate genes from our signature for in-depth functional validation. This study defines a transcriptional signature associated with palmitoylation, rather than the direct palmitoylation status. Through a series of in vitro experiments, we elucidated their mechanistic roles in driving HCC proliferation and migration, with a particular focus on the ARHGEF3-mediated activation of the YAP-RhoA signaling axis. This integrative approach from discovery to validation was undertaken precisely to bridge the identified knowledge gap and provide a novel, mechanistic framework for understanding palmitoylation's role in HCC heterogeneity and progression.

## Methods

### Datasets

Gene expression profiles and corresponding clinical data of HCC patients were systematically retrieved from three publicly accessible genomic repositories: The Cancer Genome Atlas Liver Hepatocellular Carcinoma (TCGA-LIHC), and the International Cancer Genome Consortium (ICGC) database. We first performed molecular subtyping and constructed a prognostic model using the TCGA-LIHC cohort, followed by external validation with the independent ICGC-LIRI-JP cohort. During data curation, cases lacking complete prognostic follow-up documentation (including both survival duration records and terminal event verification) were systematically excluded from the analytical cohort to ensure methodological rigor. The analytical framework incorporated collected clinical parameters encompassing survival outcomes, demographic characteristics, tumor progression markers, and genomic alteration profiles. Technical batch variations were addressed using the Combat algorithm implemented through R programming. Genomic mutation datasets were acquired from the TCGA database, providing comprehensive somatic variant information for subsequent analysis. Batch effects were corrected

using the "ComBat" algorithm with default parameters to ensure standardized and reproducible processing.

As noted in the review (https://doi.org/10.15252/embr.201846666), given that palmitoylation is primarily cat alyzed by the DHHC family of enzymes, whereas depalmitoylases mediate the reverse biological process, we chose—to maintain consistent directionality—to focus on genes positively correlated with palmitoylation. These were then intersected with the full set of genes assayed in the transcriptomic data, ultimately leading to the selection of the DHHC family members as palmitoylation-associated genes (Table S5) .

#### Consensus clustering analysis

The identified gene clusters underwent survival-based stratification through univariate Cox regression. Molecular classification of HCC cases was performed using computational algorithms from the ConsensusClusterPlus toolkit. Optimal molecular subgrouping was determined by cumulative distribution function, delta area calculations, and cluster consistency heatmap visualization. Prognostic disparities between palmitoylation-defined molecular clusters were quantified via Kaplan-Meier survival analysis implemented with the "survival" and the "survminer" R packages. The "limma" R package was employed for differential expression analysis to delineate biologically coherent gene networks associated with distinct prognostic subgroups.

#### Gene set variation analysis (GSVA) and single-sample gene set enrichment analysis (ssGSEA)

Functional pathway characterization across molecular subgroups was conducted through GSVA methodology. Reference gene collections were sourced from the latest version of the curated molecular signatures database, with differential pathway activation identified through statistical modeling frameworks. Quantitative pathway comparability assessments were conducted through ssGSEA algorithm. Cellular composition profiling was achieved by integrating lineage-specific molecular signatures into enrichment scoring systems, supported by transcriptional classification algorithms for microenvironment characterization.

#### Analysis of TME

Tumor microenvironment profiling across distinct molecular subgroups was conducted through integration of three approaches: ssGSEA, Cibersort algorithms, and Estimate scoring systems. Cellular component quantification through ssGSEA methodology was performed based on established gene signature databases. Immune cell distribution patterns were quantified using Cibersort algorithms, while stromal and immune compartment contributions were evaluated via the protocol encompassing stromal score, immune score, and combined score.

#### Prognostic signature development and validation

Following feature selection via least absolute shrinkage and selection operator (LASSO) regression, multivariate Cox proportional hazards modeling was conducted to identify survival-associated molecular signatures. A prognostic signature (Pal score) was derived through coefficient-weighted expression summation. Cohort stratification implemented median expression thresholds, delineating low-risk (Pal score < cutoff) versus high-risk (Pal score > cutoff) subgroups. Stratified survival patterns were evaluated through Kaplan-Meier methodology with log-rank testing, while temporal predictive accuracy was quantified via time-dependent receiver operating characteristic (ROC) analyses employing the survivalROC algorithm. The cut-off value for Pal score stratification was determined based on the median value. The prognostic algorithm was mathematically defined as:

$$\text{Pal score} = \sum_{n=1}^{i} (\text{Coefi} * \text{GeneExp})$$

#### Tumor mutation burden, drug susceptibility, and clinical correlation analysis

The genomic alteration profiles of HCC cases were classified into distinct categories according to Pa_ scores. Pharmacodynamic responses to conventional chemotherapeutic agents were assessed by predicting half-maximal inhibitory concentration (IC50) values. Drug sensitivity was predicted using the "pRRopheticPredict" function from the pRRophetic package. Statistical associations between palmitoylation-associated molecular signatures and clinicopathological parameters were evaluated using Pearson's chi-square test.

#### Cell culture and transfection

HCC cell models (Hep3B, Huh7, HCCLM3, MHCC-97H), liver cancer cell (SK-Hep-1) and non-malignant MIHA hepatocytes procured from Shanghai Biological Sciences Cell Repository were maintained under standardized culture conditions. Cellular proliferation was supported in controlled humidity incubators with 5% carbon dioxide atmosphere and physiological temperature conditions (37°C). Cells were maintained in DMEM supplemented with 10% fetal bovine serum. The culture medium contained 1% penicillin/streptomycin (100 U/mL penicillin and 100 µg/mL streptomycin). A final concentration of 50 nM ARHGEF3-specific gene-silencing RNA (5'-GAGACTTTCTTCATTGATC-3') and non-targeting control sequences, manufactured following standardized molecular biology protocols, were introduced into cell lines using Lipofectamine 3000 transfection

reagent (Invitrogen, Catalog: L3000001) according to manufacturer specifications. Transfection efficiency was confirmed by quantitative real-time PCR (qRT-PCR) to assess mRNA knockdown 48 h post-transfection.

#### RNA extraction and quantitative real-time PCR (qRT-PCR)

RNA isolation procedures utilized TRIzol extraction kits (Invitrogen, USA) following manufacturer guidelines. Complementary DNA synthesis preceded transcriptional quantification via real-time PCR instrumentation, with relative expression levels calculated through threshold cycle normalization methodology. Experimental workflows encompassed nucleic acid extraction from cells, reverse transcriptional processing, and subsequent amplification cycle quantification, ensuring precise measurement of target gene expression profiles. The primers are as listed: ARHGEF3 forward, 5'-AGAAGGCCAGAA AGACTCCC-3' and ARHGEF3 reverse, 5'-CAAAGCTG CTCATTGTGGGT-3'; GAPDH forward, 5'-TGCACCA CCAACTGCTTAGC-3' and GAPDH reverse, 5'-GGCA TGGACTGTGGTCATGAG-3'.

#### Immunofluorescence (IF)

Cellular preparations were processed through a standardized immunofluorescence protocol initiating with three cycles of isotonic buffer rinses (phosphate-based saline, 4 °C). Specimens were subsequently immersed in aldehyde-based fixative (4% paraformaldehyde solution) for 15 min at ambient conditions. Following triple buffer washes, membrane permeability enhancement was achieved through 0.5% nonionic surfactant treatment (10 min at room temperature). Background signal minimization involved pre-treatment with non-immune caprine serum prior to overnight cold incubation (4 °C) with primary antigen-specific antibodies. Post-primary antibody exposure, samples underwent triplicate buffer washes followed by 60-minute incubation with fluorescent secondary conjugates under controlled thermal parameters. Nuclear chromatin visualization was achieved through 5-minute application of diamidino-based fluorescent stain. High-definition fluorescence microscopy (Nikon Eclipse platform) facilitated image acquisition and documentation. The following primary antibodies were used for Western blot analysis: Anti-TR4 (ABCAM, catalog # ab137582), Anti-HIF-1α (ABCAM, catalog # ab279654), and Anti-VEGFA (ABCAM, catalog # ab52917).

#### Functional experiments

Cellular experiments were subjected to functional evaluations encompassing three key experimental methodologies: cell proliferation quantification (CCK-8) and migratory capacity assessments (scratch wound and transwell assay). For the CCK-8 assay, cell viability was measured at 0, 24, 48, 72, and 96 h after treatment. The absorbance at 450 nm was recorded following a 2-hour incubation with the CCK-8 reagent at each time point. For the scratch wound assay, a standardized scratch was created using a 200 μL sterile pipette tip to ensure a consistent initial width. The scratched area was photographed immediately after wounding (0 h) and at 48 h under a phase-contrast microscope. The migration distance was quantified using ImageJ software. For the migration assay, transwell chambers without Matrigel coating were used. After an incubation period of 24 h, cells on the lower surface were fixed, stained, and counted. These in vitro investigations were executed according to our laboratory's established experimental workflows. All cellular assays were conducted under controlled culture conditions, ensuring methodological consistency across biological replicates [21].

#### Statistical analysis

Comparisons between the two experimental groups were conducted using the nonparametric Mann-Whitney U test, while multi-group comparisons were performed using Kruskal-Wallis analysis of variance. Prognostic factors were identified through univariate and multivariate Cox proportional hazards regression models. Correlations were assessed using parametric correlation coefficients, and survival outcomes were compared with nonparametric survival curve analyses. Experimental validation was based on three independent replicates to account for both technical and biological variability. For multiple-testing correction, we applied the Benjamini-Hochberg method to control the false discovery rate (FDR). All statistical analyses were performed using R (version 4.2.1), with significance levels denoted as $^{*}p < 0.05$, $^{**}p < 0.01$, and $^{***}p < 0.001$.

## Results

#### Molecular stratification of S-palmitoylation phenotypes

The methodological framework was schematically represented in Fig. 1A. Transcriptomic divergence in S-palmitoylation regulatory genes (PRGs) between neoplastic and non-malignant hepatic tissues was visualized through principal component analysis (PCA) using TCGA-LIHC cohort data, demonstrating significant discriminatory capacity (Fig. 1B). To decipher PRG-driven molecular heterogeneity, HCC cases were partitioned into two distinct S-palmitoylation phenotypes (PAL1/PAL2) via consensus clustering (k = 2) (Fig. 1C, Figure S1A, Table S1), with cluster stability validated through cumulative distribution function analysis (Figure S1B). Patient characteristics for each cluster are presented in Table S2. Phenotypic divergence was further confirmed through complementary dimensionality reduction techniques: (1) PCA-based spatial segregation (Fig. 1D) and

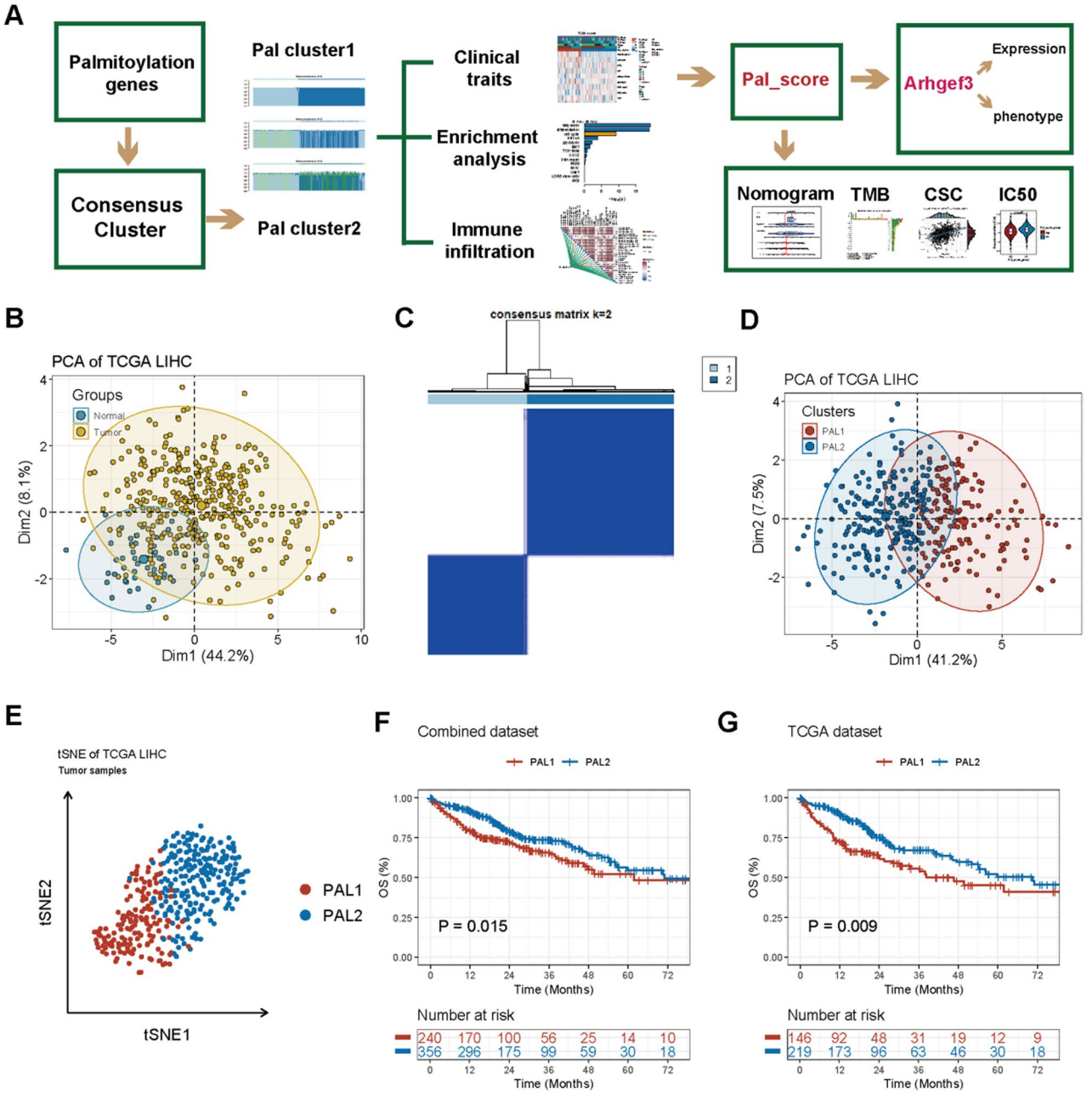


**Fig. 1** Identification of S-palmitoylation-associated genes and construction of S-palmitoylation-related clusters (PALs). **A** Comprehensive workflow diagram outlining the overall study design. **B** Palmitoylation-related genes (PRGs) effectively distinguished malignant from normal tissues. **C** Non-negative matrix factorization (NMF) clustering identified two discrete PRG-based subtypes. **D**-**E** PALs were distinguishable using PCA and t-SNE visualizations. **F**-**G** Kaplan-Meier survival curves revealed significant prognostic differences specific to PALs in both the combined cohort and TCGA-LIHC dataset

(2) t-SNE nonlinear projection (Fig. 1E), with cross-validation across TCGA-LIHC and ICGC-LIRI-JP cohorts (Figures S1C-D). Prognostic stratification revealed significant survival disparities across phenotypes-PAL1 exhibited inferior clinical outcomes compared to PAL2 in both combined database and the TCGA LIHC database (Figs. 1F-G). The differentially-expressed genes between the two PALs were shown in Table S3.

## Molecular and clinical disparities across s-palmitoylation phenotypes

Comparative analysis revealed differential overexpression of 20 PRGs in PAL1 relative to PAL2 (Fig. 2A). Hierarchical clustering demonstrated marked enrichment of pro-oncogenic processes—including cell cycle activation, EMT, and WNT/β-catenin signaling—in PAL1, whereas PAL2 exhibited preferential activation of differentiation markers and lipid metabolism pathways (Fig. 2B,

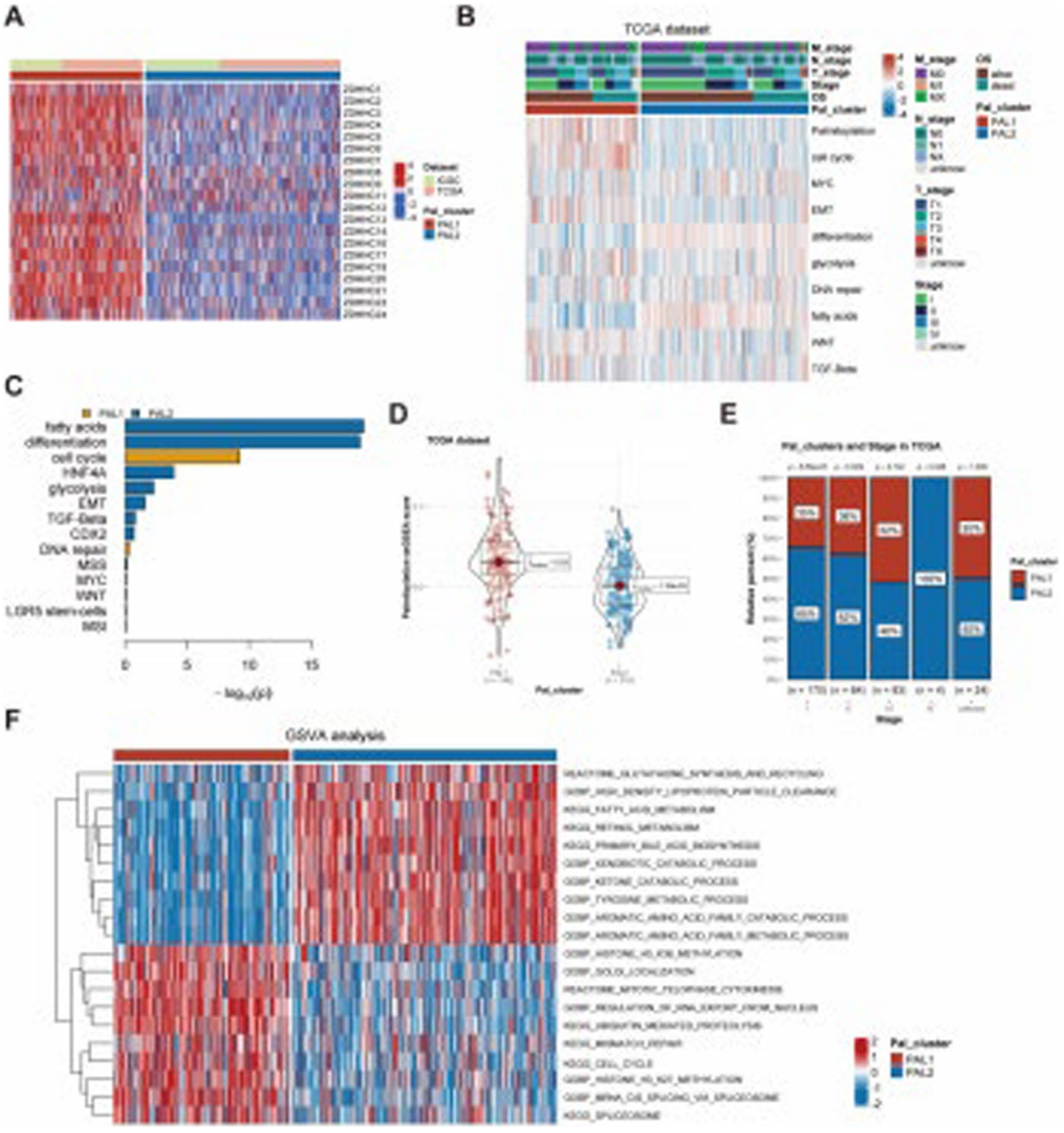


**Fig. 2** Characterization of biological and clinical attributes across PAL subtypes. **A** PRG expression profiles compared between PAL clusters. **B** Differential analysis of clinical features and 10 ssGSEA-quantified pathways distinguishing PAL subtypes. **C** Pathway enrichment comparison via GSEA between PAL clusters. **D** Comparative ssGSEA scores demonstrating superior enrichment in PAL1 versus PAL2. **E** Stage-specific distribution patterns of PAL subtypes. **F** GSVA delineating PAL subtype divergence in biological pathway activities

Figure S2A). Functional enrichment profiling identified divergent pathway activation patterns between subtypes (Fig. 2C), a dichotomy validated in the ICGC-LIRI-JP cohort (Figure S2B). ssGSEA analysis revealed differential palmitoylation activation states, with PAL1 demonstrating quantitatively superior activation metrics compared to PAL2. This phenotypic stratification established a significant inverse correlation between S-palmitoylation status and survival outcomes, identifying reduced S-palmitoylation modification as a biomarker for prolonged overall survival in multi-cohort validation (Figs. 1F-G and 2D, Figure S2D). Clinicopathological stratification of 365 TCGA-LIHC cases demonstrated stage-dependent phenotypic dominance: PAL1 prevalence escalated

from 35% (Stage I) to 52% (Stage III), inversely paralleling PAL2 depletion (65% to 48%) (Fig. 2E, Figure S2C). Mechanistically, GSVA delineated subtype-specific pathway affiliations: PAL1 exhibited hyperactivation of post-translational regulation machinery (ubiquitination, spliceosome assembly) and genomic stability networks, while PAL2 governed metabolic homeostasis through amino acid and retinoid processing (Fig. 2F).

### Immunological landscape characterization across s-palmitoylation phenotypes

Comprehensive characterization of tumor microenvironment (TME) heterogeneity across palmitoylation phenotypes was performed through integrated CIBERSORT and ssGSEA algorithms. Analytical results demonstrated distinct immune infiltration patterns, with PAL2 specimens exhibiting elevated infiltration of resting mast cells, eosinophils, and Th17 lymphocytes, coupled with reduced $CD4^+$ T cell populations across functional states relative to PAL1 (Fig. 3A and B, Figure S3A-S3B). Furthermore, ESTIMATE-based compartmentalization revealed significantly enhanced stromal, immune, and ESTIMATE scores in PAL1 cohorts (Fig. 3C). Subsequent correlation network analysis identified significant associations between palmitoylation and key immune regulators including monocytes, central memory $CD4^+$ T cells, and macrophage subsets, suggesting complex interplays between post-translational modifications and telomere maintenance mechanisms within TME niches (Fig. 3D, Figure S3C). Differential immune checkpoint expression profiles were observed, characterized by PAL1-specific upregulation of LAG3, PD-L1, and CD8A versus PAL2-predominant CD14 overexpression, indicating subtype-specific immunomodulatory potential (Fig. 3E, Figure S3D).

### Associations of PRGs with the prognosis of HCC

Prognostic modeling of HCC was conducted through randomized cohort partitioning into training and validation sets. Following filtration of survival-associated genes from PRGs, 18 candidate biomarkers were isolated through sequential LASSO regularization and multivariate Cox regression, demonstrating intersectionality with PAL-associated differential expression profiles (Fig. 4A-B, Table S4). Risk stratification using continuous prognostic signature values revealed bimodal distribution patterns, enabling dichotomization of patients into distinct prognostic categories (Fig. 4C-E, Figure S4A-B). Multivariate survival modeling established elevated signature scores as independent predictors of reduced overall survival across both derivation and validation cohorts, with alluvial mapping demonstrating significant phenotype-prognosis associations: high-risk subgroups predominantly comprised PAL1 cases demonstrating poor outcomes, whereas low-risk cohorts were enriched with PAL2 specimens exhibiting favorable trajectories (Fig. 4C and F, Figure S4B). The intricate relationship among clusters, Pal scores, and survival outcomes was depicted through an alluvial plot. A significant proportion of PAL1 exhibited high Pal scores coupled with a poor prognosis, whereas the majority of patients in PAL2 presented decreased Pal scores and appeared to experience favorable outcomes (Fig. 4G). Survival analysis and corresponding receiver operating characteristic (ROC) curves demonstrated that patients with elevated Pal scores exhibited significantly inferior clinical outcomes compared to their low Pal score counterparts in both independent cohorts (Fig. 4H and I, Figure S4D-S4E). Clinical translation was achieved through nomogram construction integrating TNM staging and signature scores, demonstrating superior 60-month survival prediction accuracy versus conventional staging systems, with calibration plots confirming high concordance between predicted and observed 1-/3-/5-year outcomes (Fig. 5A and E).

### Prognostic signature associations with clinicopathological variables and TMB in HCC

Analytical evaluation of prognostic signature correlations with clinicopathological parameters revealed a progressive elevation of risk stratification metrics (Pal scores) across advanced tumor stages (Fig. 6A). Cellular stemness potential, quantified through stemness index (CSC) profiling, demonstrated significant positive covariation with prognostic signature values (Fig. 6B). TMB analysis identified a proportional relationship with risk stratification tiers, which may indicate a potential for increased immunotherapy benefit in high-risk subgroups (Fig. 6C). Mutational landscape visualization via waterfall plots delineated differential genomic alteration patterns across risk groups (Fig. 6D and E). Furthermore, drug sensitivity analysis suggested that patients with low Pal scores could show greater responsiveness to cyclopamine, sorafenib, gemcitabine, cisplatin, rapamycin, and etoposide, whereas gefitinib and metformin might exhibit superior therapeutic efficacy in those with elevated Pal scores (Fig. 6F), informing phenotype-specific therapeutic stratification. These findings are hypothesis-generating and highlight potential associations that warrant further experimental and clinical validation.

### Validation of the role of ARHGEF3 in HCC

Following the screening of genes in the aforementioned prognostic model label, ARHGEF3 was selected as the target gene due to its position among the top three genes with the highest coefficient values and its previously unelucidated role in hepatocellular carcinoma. Initial qRT-PCR analysis demonstrated significantly elevated ARHGEF3 expression levels in common HCC and liver

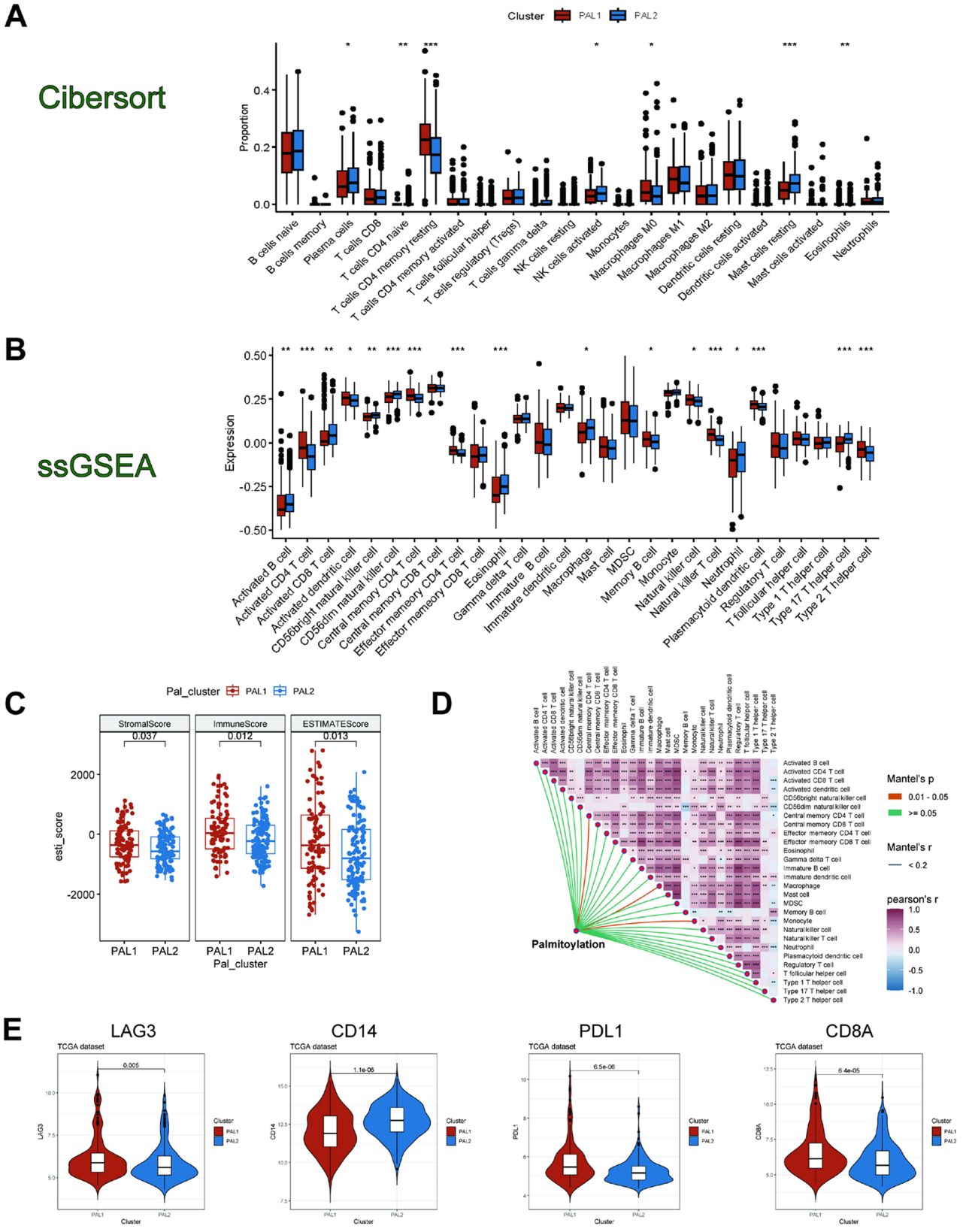


**Fig. 3** TME characterization across PAL subtypes. **A** CIBERSORT deconvolution quantified immune cell infiltration levels in PAL clusters using LM22 signatures. B ssGSEA-derived immune cell abundance profiles within PAL subtypes. **C** ESTIMATE algorithm assessment of immune-stromal heterogeneity among PALs. **D** Association mapping of S-palmitoylation patterns across diverse immune cell populations. **E** Differential expression patterns of LAG3, CD14, PD-L1 (CD274), and CD8A between PAL subtypes

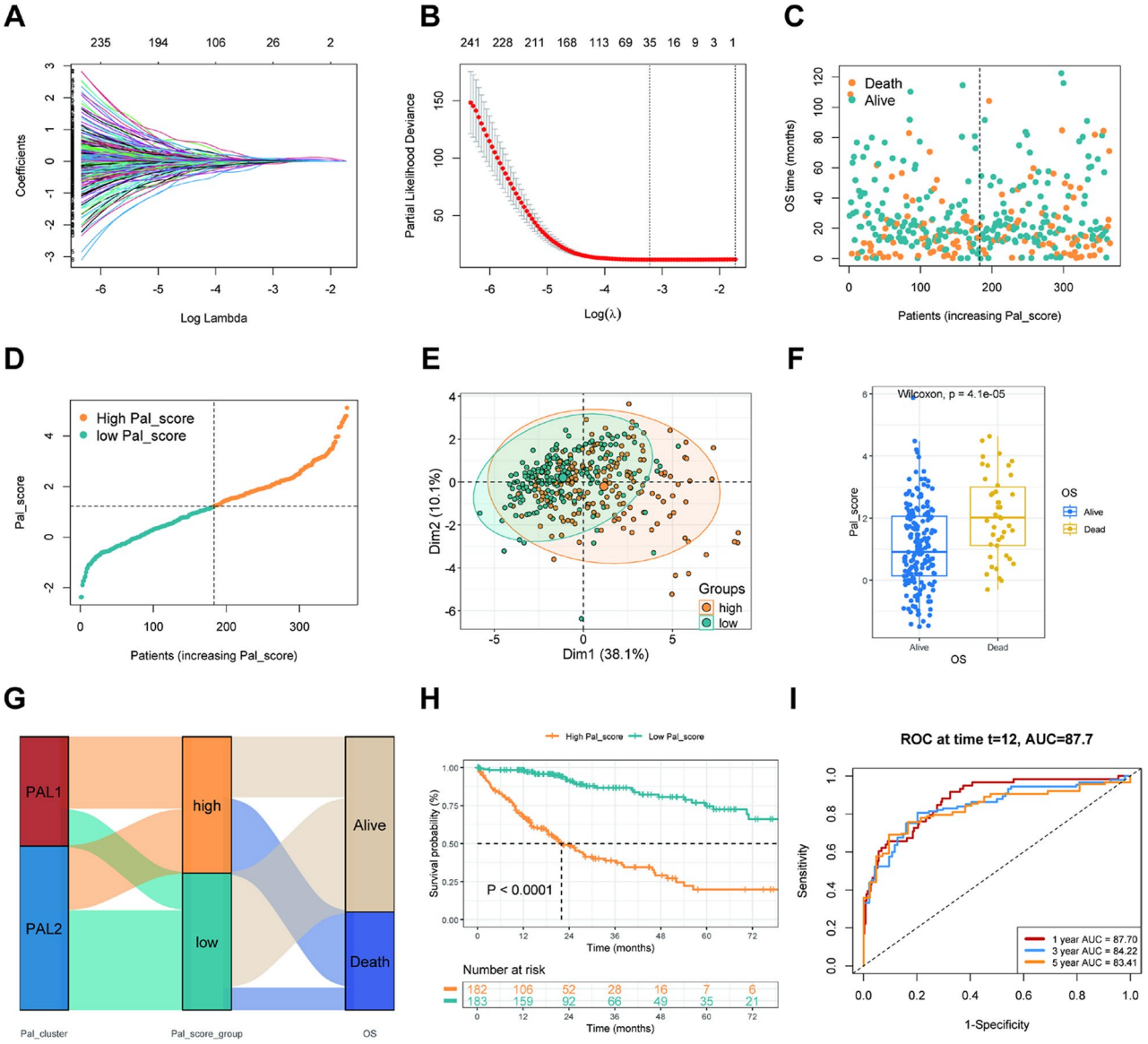


**Fig. 4** Development and clinical validation of the Pal scoring system. **A**-**B** LASSO regression identified 18 prognostic genes for subsequent multivariate Cox analysis. **C**-**D** Pal score distribution stratified by patient survival status. **E** PCA visualization revealed distinct separation between high and low Pal score cohorts. **F** Comparative Pal score analysis across HCC clinical outcome groups. **G** Sankey diagram mapping patient trajectories across molecular clusters. **H**-**I** Kaplan-Meier survival stratification by Pal scores and corresponding ROC curve analysis for prognostic accuracy

cancer cell lines compared to the normal hepatic epithelial cell line MIHA (Fig. 7A). Consequently, functional experiments were conducted in Huh7 and Hep3B cells, which exhibited the highest ARHGEF3 expression, utilizing short hairpin RNA for knockdown and plasmid vectors for overexpression (Fig. 7B). Regarding the expression levels in tissues, ARHGEF3 showed high expression in 64 HCC tissues and low expression in 16 HCC tissues, with a statistically significant difference (Fig. 7C). Assessments of proliferative and migratory capacities via CCK-8 assay, scratch wound healing assay, and transwell assay revealed that ARHGEF3 knockdown attenuated these capabilities, whereas overexpression enhanced them (Fig. 7D and F). Investigation into the mechanistic basis of ARHGEF3's biological function considered prior evidence implicating ARHGEF3 in obesity regulation through activation of the YAP-RhoA and PPARγ pathways, with the YAP-RhoA axis recognized as a significant contributor to HCC progression [22–24]. Protein-protein interaction prediction using the STRING online tool indicated a significant association between ARHGEF3 and RhoA (Fig. 7G and H). Subsequent immunofluorescence analysis demonstrated that expression levels of the YAP-RhoA axis positively correlated with ARHGEF3 expression levels in cells with modulated ARHGEF3 expression. These collective findings suggest

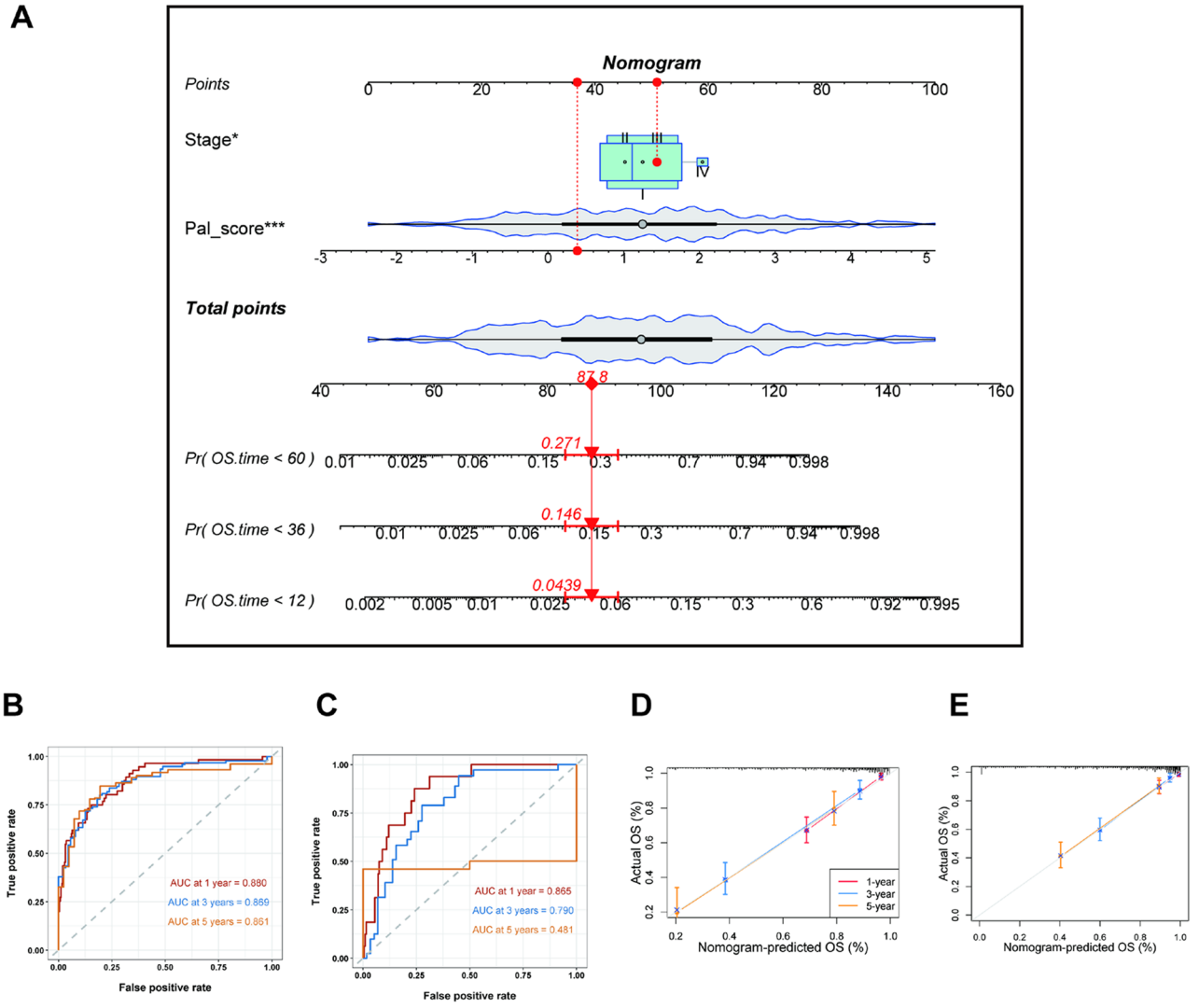


**Fig. 5** Development and validation of a clinical nomogram. **A** Graphical representation of the prognostic nomogram. **B**-**C** ROC curve analysis assessing predictive discrimination in training and test cohorts. **D**-**E** Calibration performance evaluation across derivation and validation datasets

that ARHGEF3 likely regulates HCC proliferation and migration via the YAP-RhoA axis (Fig. 7I). We utilized GPS-Palm (https://doi.org/10.1093/bib/bbaa038) to pred ict the palmitoylation sites of ARHGEF3, and the prediction results are provided in Supplementary Table S6.

## Discussion

HCC continues to pose significant therapeutic challenges despite advances in systemic therapies. While immune checkpoint inhibitors combined with anti-angiogenic agents have improved survival in advanced HCC, primary and acquired resistance remains prevalent. This therapeutic impasse underscores the urgent need for molecular subtyping frameworks that can guide precision interventions. Our study addresses this gap by investigating protein S-palmitoylation – a dynamically reversible post-translational modification – as a novel regulator of HCC heterogeneity. The field has increasingly recognized palmitoylation's multifaceted roles in oncogenesis, where it modulates diverse processes from RAS membrane localization to PD-L1 stabilization across cancer types [25]. Yet its systematic exploration in HCC pathogenesis, particularly regarding TME interactions and clinical stratification, has remained limited despite reports implicating PCSK9, FASN, and AEG-1 palmitoylation in HCC progression [18, 20, 26].

Our analysis revealed two fundamentally distinct S-palmitoylation phenotypes (PAL1 and PAL2) with profound clinical implications. The PAL1 phenotype, characterized by coordinated overexpression of 20 PRGs, demonstrated strong associations with advanced tumor stages and inferior survival outcomes across both TCGA and ICGC cohorts. This aggressive phenotype exhibited molecular hallmarks of malignancy including enhanced

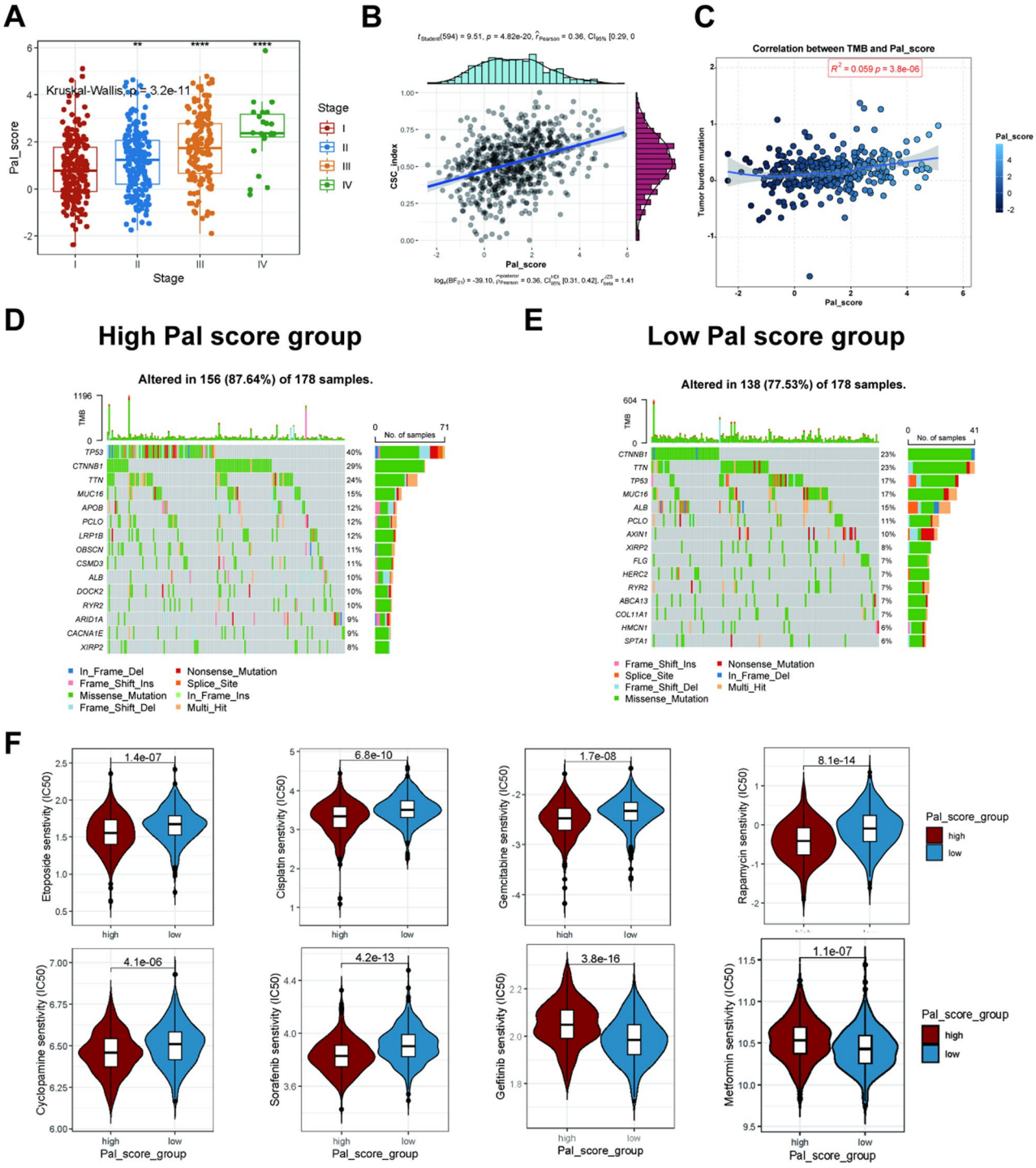


**Fig. 6** Comparative profiling of high versus low Pal score cohorts. **A** Association between Pal scores and advancing clinical tumor stages. **B** Correlation mapping of Pal scores against cancer stem cell (CSC) indices. **C**-**E** TMB relationships stratified by Pal score groups. **F** Pharmacological sensitivity analysis (IC50) revealing differential drug responses across Pal score classifications

cell cycle progression, epithelial-mesenchymal transition, and Wnt/β-catenin signaling activation. Conversely, the PAL2 cluster showed preferential lipid metabolic pathway activation and significantly better prognosis. Crucially, this molecular stratification transcends conventional staging systems. The divergent TME landscapes further validate this classification: PAL1 tumors displayed immunosuppressive signatures with elevated PD-L1/LAG3 expression and $CD8^{+}$ T-cell exhaustion, whereas PAL2 microenvironments featured enhanced mast cell and

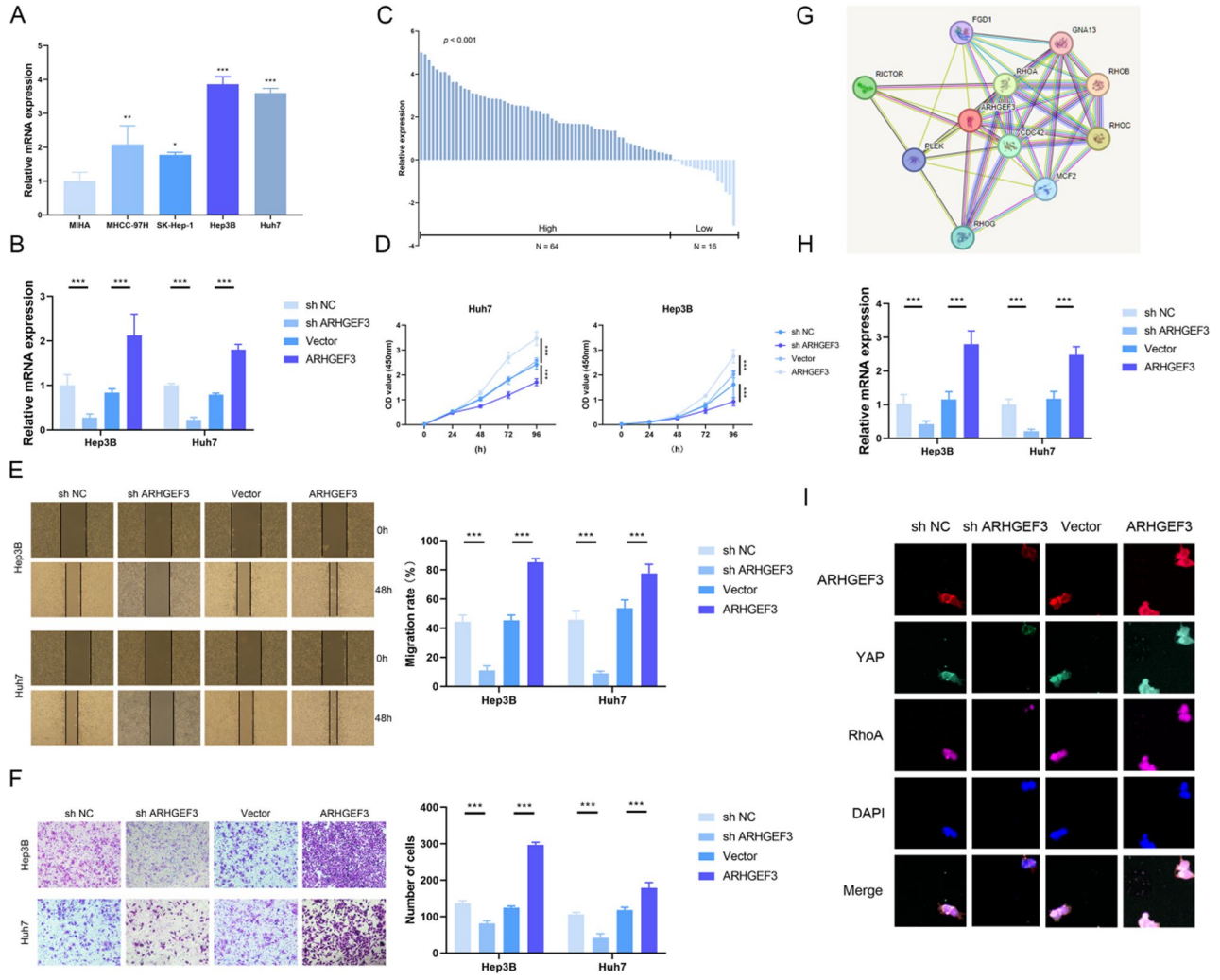


**Fig. 7** ARHGEF3 upregulation drives HCC malignancy in vitro. **A** RT-qPCR quantification of ARHGEF3 expression in HCC cell lines versus normal hepatocyte MIHA controls. **B** Validation of ARHGEF3 knockdown (via shRNA) and overexpression (via plasmid) efficiency in Hep3B and Huh7 cells. **C** RT-qPCR revealed significantly higher ARHGEF3 expression in HCC tissues than in adjacent non-tumor tissues. **D** CCK-8 assays assessing proliferation kinetics after ARHGEF3 modulation. **E**-**F** Cell migration evaluated by wound-healing (**E**) and transwell (**F**) assays following ARHGEF3 manipulation. **G** Protein-protein interaction network of ARHGEF3 predicted by STRING. **H** Immunoblot analysis of YAP expression changes upon ARHGEF3 perturbation. **I** Immunofluorescence visualization of YAP–RhoA axis activation in ARHGEF3-modified Hep3B cells

Th17 infiltration. These findings position palmitoylation as a master regulator of both tumor-intrinsic malignancy and immune evasion mechanisms. Compared with existing research, our work offers distinctive advances: we developed a clinically applicable nomogram integrating prognostic factors and analyzed subtype-specific drug vulnerabilities; maintained rigorous logical coherence by constructing all subsequent models directly from subtype-derived differential genes; and provided deeper mechanistic insights by validating the functional role of key targets through the YAP-RhoA axis. Therefore, beyond encompassing previous analytical frameworks, our study enhances clinical translatability, logical consistency, and mechanistic depth, offering renewed perspectives on the role of palmitoylation in hepatocellular carcinoma.

Building upon this molecular taxonomy, we developed and validated the Pal score—a quantitative prognostic signature derived from survival-critical palmitoylation-related genes (PRGs). This continuous risk metric demonstrated significant clinical value by independently predicting overall survival beyond conventional clinicopathological parameters. The Pal score also showed strong biological coherence, with higher scores correlating with advanced tumor stage, increased tumor mutational burden, and elevated cancer stemness indices. Its clinical translatability was further reinforced through integration into a nomogram, which significantly outperformed TNM staging in predicting 5-year survival.

In terms of drug response, tumors with low Pal scores exhibited heightened sensitivity to sorafenib and conventional chemotherapeutics, whereas high-score tumors showed differential responsiveness to targeted agents such as gefitinib. This functional stratification offers a practical guide for phenotype-specific therapy selection. Furthermore, the PAL1/PAL2 subtypes, while possibly overlapping with certain established molecular features, provide a biologically distinct and mechanistically informative classification by directly linking tumor biology to the palmitoylation regulatory machinery. Together, this framework not only complements existing stratification systems but may also help explain tumor heterogeneity through a novel molecular lens, potentially revealing therapeutic targets that transcend conventional classification boundaries.

Regarding the role of ARHGEF3, although our in silico predictions suggest multiple putative palmitoylation sites, these remain to be experimentally confirmed. We recognize that site-directed mutagenesis of these cysteine residues and the systematic screening of the ZDHHC enzyme family are required to establish the palmitoylation-dependence of ARHGEF3. Such experiments would provide more definitive evidence of how palmitoylation modulates ARHGEF3 function. Furthermore, while we observed a correlation between ARHGEF3 and the YAP-RhoA signaling axis, our current evidence is largely supportive and descriptive. The immunofluorescence data, while suggestive, do not establish a causal link. Future studies involving pathway-specific inhibitors and functional rescue assays are warranted to confirm whether the YAP-RhoA axis is the primary functional requirement for ARHGEF3-driven HCC progression. These future directions will be essential to translate our computational and preliminary experimental findings into concrete therapeutic strategies.

The innovative dimensions of this work are threefold. First, we established the palmitoylation-based molecular classification of HCC that integrates TME profiling with clinical outcomes. Second, the Pal score constitutes a novel precision medicine tool capable of predicting both prognosis and therapeutic vulnerability. Third, our mechanistic dissection of ARHGEF3 uncovered a previously unrecognized palmitoylation-YAP-RhoA regulatory axis. These advances position palmitoylation modulation as a promising therapeutic strategy complementary to existing modalities.

However, several limitations of this study should be acknowledged. Our investigation focuses on a palmitoylation-associated transcriptional signature inferred from transcriptomic data, whose underlying biomolecular mechanisms currently lack experimental validation. The proposed molecular subtyping system requires validation in prospective, multi-ethnic cohorts to account for population heterogeneity. Although the Pal score demonstrates robust prognostic performance, its clinical translation depends on the development of standardized assays. In fact, ARHGEF3 is predicted to be palmitoylated, rather than experimentally validated as such. While the functional role of ARHGEF3 has been established, its specific palmitoylation sites and the corresponding modifying enzymes remain to be characterized. Future studies should employ acyl-biotin exchange proteomics to comprehensively map palmitoylome dynamics across subtypes, investigate the crosstalk between palmitoylation and ubiquitination in regulating YAP–RhoA signaling, and validate combination therapeutic strategies targeting palmitoylation networks using patient-derived xenograft models. Moreover, there are several limitations in our study methodology that warrant improvement, such as the absence of in vivo experimental validation and heavy reliance on public datasets. Finally, the palmitoylation activity characterized in this study is inferred from transcriptomic profiles. While gene expression provides a high-throughput view of the regulatory landscape, it may not perfectly mirror the functional palmitoylation flux. Future investigations should employ biochemical gold standards, such as acyl-biotin exchange (ABE) or palmitoyl-proteomics, to directly quantify protein modification levels and validate our transcriptomic findings at the post-translational level.

## Conclusions

This investigation defines distinct HCC molecular subtypes derived from palmitoylation modification profiles, alongside a comprehensive analysis of associated clinicopathological traits and TME constituents for each subtype. We developed a novel prognostic signature (termed Pal score) for predicting outcomes in HCC patients. Experimental validation pinpointed ARHGEF3 as a pivotal oncogenic driver, demonstrating marked overexpression in HCC tissues and functionally driving tumor advancement. These findings establish a molecular taxonomy that facilitates precision diagnostics and guides the development of targeted therapies against this malignancy.

### Abbreviations

| | |
|---|---|
| PALs | S-palmitoylation-associated clusters |
| TME | Tumor microenvironment |
| TMB | Tumor mutation burden |
| PRGs | S-palmitoylation-related genes |

## Supplementary Information

The online version contains supplementary material available at https://doi.org/10.1186/s12920-026-02356-z.

Supplementary Material 1. Supplementary Figure S1. (A) The heat map of consensus clusters (k= 3-6). (B) The CDF and delta index of consensus clustering. k is the number of clusters when using consensus clustering.

(C) PALs were distinguishable using PCA visualizations according to the ICGC-LIRI-JP databae. (D) PALs were distinguishable using t-SNE visualizations according to the ICGC-LIRI-JP databae. Supplementary Figure S2. (A) Differential analysis of clinical features and 10 ssGSEA-quantified pathways distinguishing PAL subtypes. (B) Pathway enrichment comparison via GSEA between PAL clusters. (C) Stage-specific distribution patterns of PAL subtypes. (D) Comparative ssGSEA scores demonstrating superior enrichment in PAL1 versus PAL2. Supplementary Figure S3. (A) Cibersort analysis revealed the proportion of immune cells present in PALs. (B) The ssGSEA analysis demonstrated the varying infiltration levels of immune cells in PALs. (C) Association mapping of S-palmitoylation patterns across diverse immune cell populations. (D) Differential expression of LAG3, CD14, PD-L1 (CD274), and CD8A in PALs. Supplementary Figure S4. (A-B) Distribution of Pal scores in patients with different OS status in the ICGC-LIRI-JP database. (C) PCA analysis exhibited the distribution between the high and low Pal score groups in the ICGC-LIRI-JP database. (D) Patients in the ICGC-LIRI-JP database with dead status attained significantly elevated TM scores. (E) Survival analysis employing the effective AUC demonstrated that the cohort with elevated TM scores exhibited a significantly poorer prognosis within the test set.

Supplementary Material 2.

**Acknowledgements**
Not applicable.

**Authors' contributions**
BQ X: Formal analysis, Visualization, Writing-Original Draft, Supervision, Project administration. JL D: Methodology, Formal Analysis, Investigation, Writing-review & Editing, Validation, Data Curation. Z C: Conceptualization, Supervision, Resources.

**Funding**
Not applicable.

**Data availability**
Publicly available datasets were analyzed in this study. These data can be found here: https://www.cancer.gov/about-nci/organization/ccg/research/structural-genomics/tcga, https://www.ncbi.nlm.nih.gov/gds/ and https://dcc.icgc.org/.

## Declarations

**Ethics approval and consent to participate**
Not applicable.

**Competing interests**
The authors declare no competing interests.

Received: 30 August 2025 / Accepted: 26 March 2026
Published online: 02 April 2026

**References**

1. Siegel RL, Miller KD, Wagle NS, Jemal A. Cancer statistics, 2023. CA-Cancer J Clin. 2023;73(1):17–48.
2. Lv KJ, Yu SZ, Wang Y, Zhang SR, Li WY, Hou J, Tan DL, Guo H, Hou YZ. Cancer-associated fibroblasts promote the progression and chemoresistance of HCC by inducing IGF-1. Cell Signal. 2024;124:13.
3. Peng YF, Shi YH, Ding ZB, Ke AW, Gu CY, Hui B, Zhou J, Qiu SJ, Dai Z, Fan J. Autophagy inhibition suppresses pulmonary metastasis of HCC in mice via impairing anoikis resistance and colonization of HCC cells. Autophagy. 2013;9(12):2056–68.
4. Lothrop AP, Torres MP, Fuchs SM. Deciphering post-translational modification codes. FEBS Lett. 2013;587(8):1247–57.
5. Fhu CW, Ali A. Protein Lipidation by Palmitoylation and Myristoylation in Cancer. Front Cell Dev Biol. 2021;9:15.
6. Ko PJ, Dixon SJ. Protein palmitoylation and cancer. EMBO Rep. 2018;19(10):14.
7. Jiang H, Zhang XY, Chen X, Aramsangtienchai P, Tong Z, Lin HN. Protein Lipidation: Occurrence, Mechanisms, Biological Functions, and Enabling Technologies. Chem Rev. 2018;118(3):43–112.
8. Greaves J, Chamberlain LH. Palmitoylation-dependent protein sorting. J Cell Biol. 2007;176(3):249–54.
9. Barylko B, Mao YS, Wlodarski P, Jung G, Binns DD, Sun HQ, Yin HL, Albanesi JP. Palmitoylation Controls the Catalytic Activity and Subcellular Distribution of Phosphatidylinositol 4-Kinase IIα. J Biol Chem. 2009;284(15):9994–10003.
10. Heakal Y, Woll MP, Fox T, Seaton K, Levenson R, Kester M. Neurotensin receptor-1 inducible palmitoylation is required for efficient receptor-mediated mitogenic-signaling within structured membrane microdomains. Cancer Biol Ther. 2011;12(5):427–35.
11. Zhou B, Liu L, Reddivari M, Zhang XA. The palmitoylation of metastasis suppressor KAI1/CD82 is important for its motility- and invasiveness-inhibitory activity. Cancer Res. 2004;64(20):7455–63.
12. Marjon KD, Termini CM, Karlen KL, Saito-Reis C, Soria CE, Lidke KA, Gillette JM. Tetraspanin CD82 regulates bone marrow homing of acute myeloid leukemia by modulating the molecular organization of N-cadherin. Oncogene. 2016;35(31):4132–40.
13. Amendola C. Kras4a Directly Regulates Hexokinase 1. 2020.
14. Tong HY, Yu XG, Lu XC, Wang P. Downregulation of solute carriers of glutamate in gliosomes and synaptosomes may explain local brain metastasis in anaplastic glioblastoma. IUBMB Life. 2015;67(4):306–11.
15. Klaus C, Schneider U, Hedberg C, Schütz AK, Bernhagen J, Waldmann H, Gassler N, Kaemmerer E. Modulating effects of acyl-CoA synthetase 5-derived mitochondrial Wnt2B palmitoylation on intestinal Wnt activity. World J Gastroenterol. 2014;20(40):14855–64.
16. von Karstedt S, Montinaro A, Walczak H. Exploring the TRAILs less travelled: TRAIL in cancer biology and therapy. Nat Rev Cancer. 2017;17(6):352–66.
17. Mansilla F, Birkenkamp-Demtroder K, Kruhoffer M, Sorensen FB, Andersen CL, Laiho P, Aaltonen LA, Verspaget HW, Orntoft TF. Differential expression of DHHC9 in microsatellite stable and instable human colorectal cancer subgroups. Br J Cancer. 2007;96(12):1896–903.
18. Sun Y, Zhang H, Meng JP, Guo F, Ren DY, Wu HS, Jin X. S-palmitoylation of PCSK9 induces sorafenib resistance in liver cancer by activating the PI3K/AKT pathway. Cell Rep. 2022;40(7):22.
19. Mo YQ, Han YM, Chen Y, Fu CL, Li Q, Liu Z, Xiao MM, Xu B. ZDHHC20 mediated < i > S-palmitoylation of fatty acid synthase (FASN) promotes hepatocarcinogenesis. Mol Cancer. 2024;23(1):20.
20. Zhou BH, Wang Y, Zhang LC, Shi XY, Kong HS, Zhang MJ, Liu Y, Shao X, Liu ZL, Song HX, et al. The palmitoylation of AEG-1 dynamically modulates the progression of hepatocellular carcinoma. Theranostics. 2022;12(16):6898–914.
21. Zhang X, Wang S, Wang HX, Cao JC, Huang XX, Chen Z, Xu PH, Sun GL, Xu JH, Lv JL, et al. Circular RNA circNRIP1 acts as a microRNA-149-5p sponge to promote gastric cancer progression via the AKT1/mTOR pathway. Mol Cancer. 2019;18:24.
22. Khaliq SA, Park S-Y, Maham S, Cho Y, Lee M, Nam S, Seong JK, Chen J, Choi CS, Yoon M-S. ARHGEF3 coordinates adipocyte hypertrophy and differentiation through dual YAP-RhoA and PPARgamma activation. J Adv Res. 2025.
23. Liu YC, Zhuo S, Zhou YX, Ma LC, Sun ZH, Wu XL, Wang XW, Bin G, Yang YZ. Yap-Sox9 signaling determines hepatocyte plasticity and lineage-specific hepatocarcinogenesis. J Hepatol. 2022;76(3):652–64.
24. Fu LS, Wang XY, Yang Y, Chen MH, Kuerban A, Liu HJ, Dong YW, Cai QQ, Ma MZ, Wu XZ. Septin11 promotes hepatocellular carcinoma cell motility by activating RhoA to regulate cytoskeleton and cell adhesion. Cell Death Dis. 2023;14(4):15.
25. Liu Z, Xiao MM, Mo Y, Wang H, Han YM, Zhao X, Yang X, Liu ZX, Xu B. Emerging roles of protein palmitoylation and its modifying enzymes in cancer cell signal transduction and cancer therapy. Int J Biol Sci. 2022;18(8):3447–57.
26. Liu J, Shen YY, Liu J, Xu DD, Chang CY, Wang JM, Zhou JS, Haffty BG, Zhang LJ, Bargonetti J, et al. Lipogenic enzyme FASN promotes mutant p53 accumulation and gain-of-function through palmitoylation. Nat Commun. 2025;16(1):18.

## Publisher's Note